Characteristic multi-wavelength emission signatures from strong shock-shock interactions in perturbed relativistic jets

γ 2022
7th Heidelberg International Symposium on
High Energy Gamma-Ray Astronomy
Barcelona, July 4-8 2022

Gaëtan Fichet de Clairfontaine[1], Zakaria Meliani[1], and Andreas Zech[1]

[1]LUTh - Observatoire de Paris, Université PSL, Université Paris Cité, CNRS

Abstract

The diffusive shock acceleration of a population of relativistic electrons on internal shocks is one of the main scenarios to account for the multi-wavelength (MWL) flux variability observed in relativistic jets of active galactic nuclei. In addition to observations of flux variability, constraints are also provided by very-long-baseline interferometry (VLBI), which shows a large variety of moving and standing emission zones with distinct behavior.

We will present a model combining relativistic magneto-hydrodynamic jet simulations (`MPI-AMRVAC` code) with radiative transfer (`RIPTIDE` code). We simulate the evolution of standing and moving emission zones in the jet and study their MWL signatures from the radio to the X-ray band by taking into account relativistic effects (Doppler beaming and light crossing effect (LCE)).

We focus our attention on strong interactions between a fast moving shock and stationary recollimation shocks, to study how such events lead to a significant perturbation of the stationary jet structure.

Sufficiently strong shock - shock interactions lead to the appearance of trailing components, which appear in the wake of the leading moving shock. We characterize such relaxation shocks by two observational markers, one the *fork pattern* is visible in the radio band in the time-distance plot of bright VLBI components and one at higher frequencies under the form of *flare echoes*. Our results provide a coherent interpretation of radio VLBI observations in several radio galaxies.

Jet and radiative modeling

`MPI-AMRVAC` (*Message-Passing Interface Adaptive Mesh Refinement Advection Code*) (*1*) :

Input : ambient medium, jet and ejecta initial conditions.

- Shock detection method visible in (*2*) where the electrons fluid is injected;
- Evolution of the electrons fluid upper cutoff Lorentz factor $\gamma_{\rm e,max}$ (*3*) where synchrotron radiative cooling is taken into account;
- The turbulent magnetic field strength $B_{\rm turb}$ is set as a fraction of 1% of the thermal energy and evolved in time in the fluid.

Output : 2D save states of the jet fluid and electron fluid.

`RIPTIDE` code (*Radiation and Integration Processes with Time Dependence*) (*4*, *5*):

Input : 2D save states from `MPI-AMRVAC`, observation angle $\theta_{\rm obs}$ and frequency ν.

- Computation of the synchrotron emissivity and absorption parameters in each cell following approximations proposed by (*6*);
- Transformation imposed by relativistic effects such as Doppler beaming and light crossing effect (LCE) following method proposed by (*7*);
- Resolution of the radiative transfer equation along a given line of sight for an observer and computation of the observed synchrotron flux.

Output : 2D synchrotron maps as observed at the frequency ν.

Jet setup

Our relativistic jet is,

- ➜ cylindrical and supersonic;
- ➜ in over-pressure (*8*) compared to a static and uniform ambient medium (AM);
- ➜ subject to a perturbation (ejecta);
- ➜ set with $L_{\rm kin} = 10^{46}$ erg.s^{-1} the total kinetic luminosity (*9*) and $R_{\rm jet} = 0.1$ pc the jet radius (*10*).

Component	ρ (cm^{-3})	p (dyn $\cdot$ cm^{-2})	γ
AM	10^3	1	1
jet	0.1	1.5	3
ejecta	0.1	1.5	24

Table 1: Parameters used in simulation.

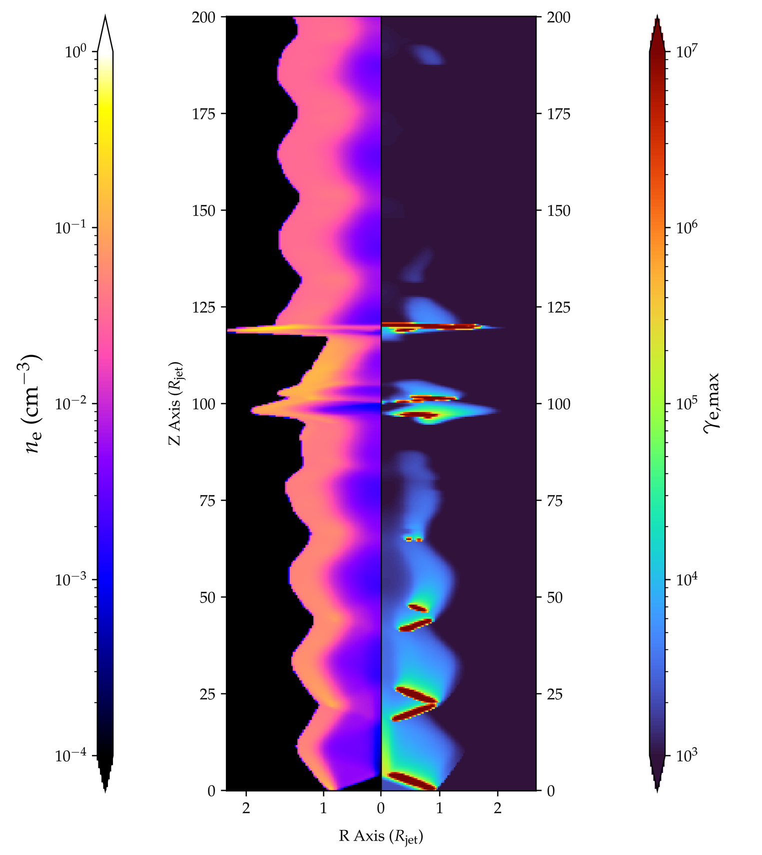

Figure 1: Electron number density n_e and $\gamma_{\rm e,max}$ in the jet. The main perturbation is located around 120 $R_{\rm jet}$ following by a relaxation shock.

Observational markers of relaxation shocks

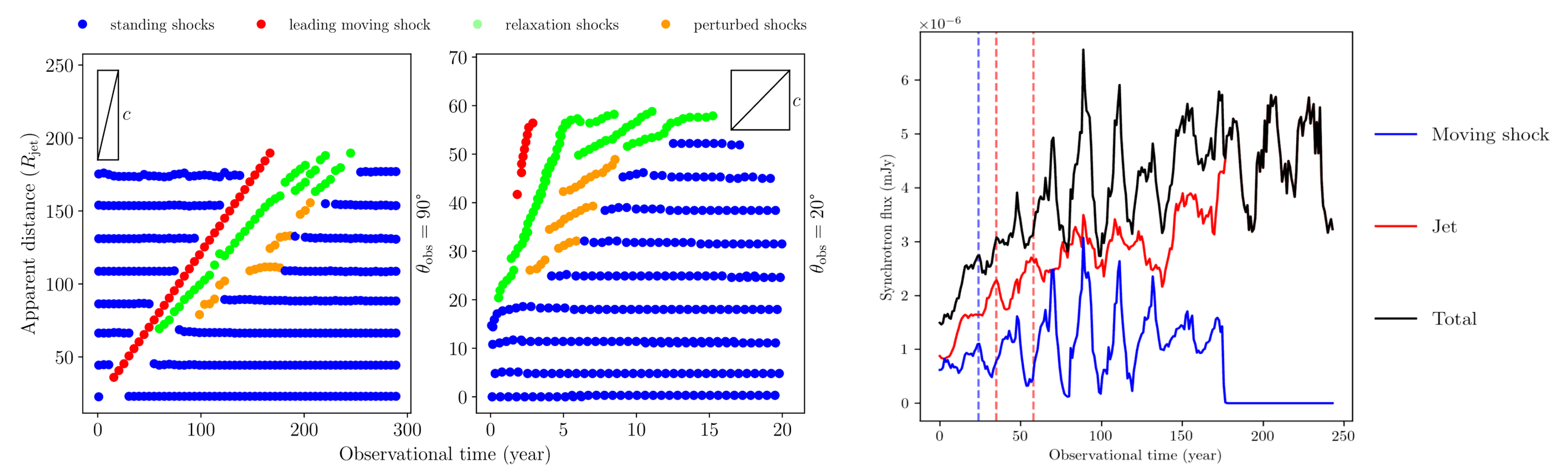

Figure 2: **Left :** Apparent distance traveled by standing and moving knots in time (see legend). We display here results with LCE for $\theta_{\rm obs} = 90°$ and $\theta_{\rm obs} = 20°$ at $\nu = 10^{10}$ Hz. **Right :** Light curves with flux origin (see legend) obtained at $\theta_{\rm obs} = 90°$ and for $\nu = 10^{18}$ Hz.

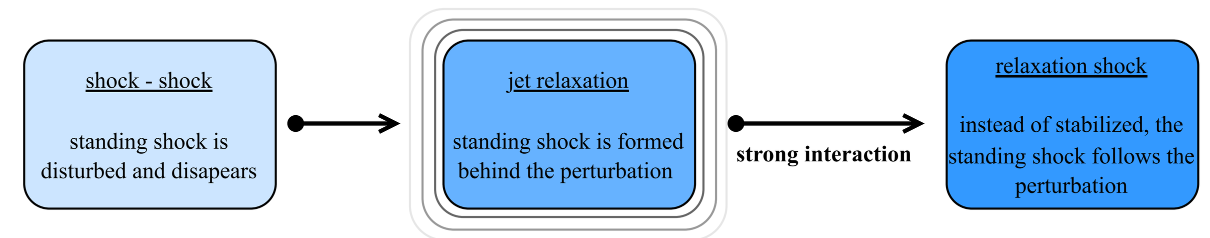

The fork pattern

- ➨ is visible in the radio band in apparent distance vs. time plot;
- ➨ is formed by (at least) three branches;
- ➨ show superluminal motions for low $\theta_{\rm obs}$ (Fig. 2, left);
- ➩ allows to constraint the apparent speed of the jet.

The flare echo

- ➨ is visible at higher frequencies (X band) due to a fast synchrotron cooling;
- ➨ is associated to a remnant emission of perturbed standing shock and/or relaxation shock (Fig. 2, right);
- ➩ allows to probe the standing shock structure through the small flaring scale.

Application to 3C 111

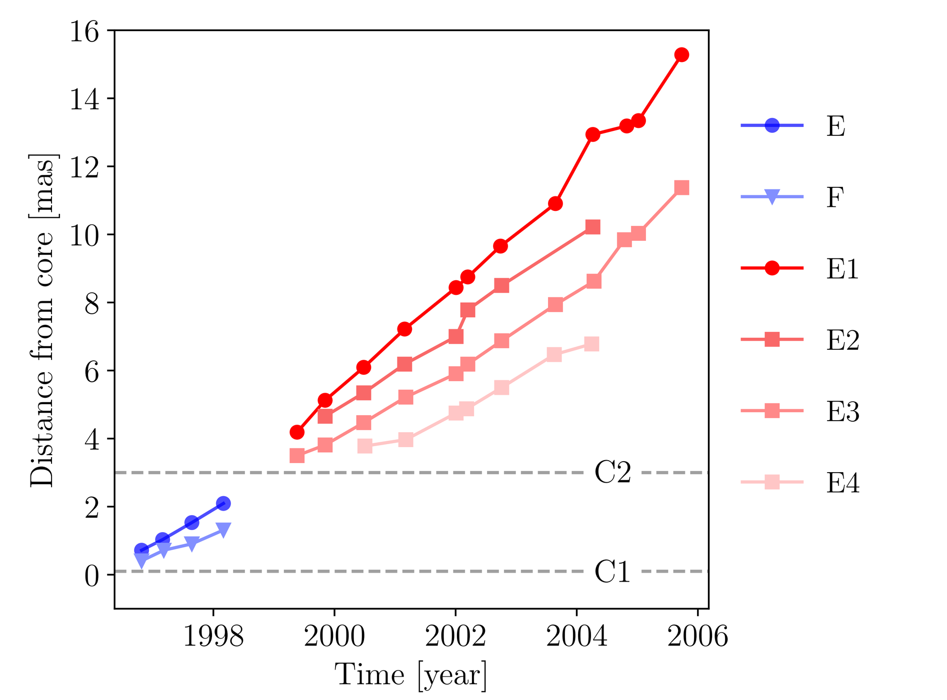

Figure 3: Core separation of components vs. time plot adapted from (*11*) observed with the VLBA 2 cm Survey and MOJAVE monitoring programs.

- ➨ 3C 111 is a FR II type AGN where trailing components have been observed by (*11*) correlated with standing radio nodes (**C1** & **C2**) (respectively at 0.1 and 3 mas from the radio core) (*12*, *13*) (Fig. 3).

Our scenario

- ➩ Fork patterns are visible on two different periods with similar observed behaviors in simulations positioned on standing shocks;
- ➩ First event: drift of a perturbed standing shock (**C1** → **F**) after interaction with a leading one (**E**) (Fig. 2, left);
- ➩ Second event: propagation of several relaxation shocks (**E2**, **E3** & **E4**) after interaction between **C2** and **E1** (**E** → **E1**).

Conclusion and prospects

- ✓ Simulations of strong shock - shock interactions lead to a great variety of emission regions;
- ✓ Two observational markers of relaxation shocks : ***fork events*** and ***flare echoes*** are victims of observational limitations (spatial and temporal resolution);
- ✓ Comparison with 3C 111 seems promising, our scenario may be applied to other sources;
- ✓ Characterization of relaxation shocks can help us to constrain the jet physics and to test the likelihood of the "shock - shock" scenario.

- ☛ Addition of the synchrotron polarization;
- ☛ Simulations of more complex jets (dedicated simulations on M 87 jet) and the reproduction of the MWL (radio to VHE γ → SSC implemented!) broadband emission and variability associated with a standing shock (as HST-1 in M 87 in 2005).

SCAN ME
Scan to see the associated article!

References

1. R. Keppens *et al.*, *JCP* **231**, 718–744 (Feb. 2012).
2. O. Zanotti, L. Rezzolla, L. Del Zanna, C. Palenzuela, *A&A* **523**, A8 (Nov. 2010).
3. H. J. van Eerten, K. Leventis, Z. Meliani, R. A. M. J. Wijers, R. Keppens, *MNRAS* **403**, 300–316 (Mar. 2010).
4. G. Fichet de Clairfontaine, Z. Meliani, A. Zech, O. Hervet, *A&A* **647**, A77 (Mar. 2021).
5. G. Fichet de Clairfontaine, Z. Meliani, A. Zech, *A& A* **661**, A54 (May 2022).
6. K. Katarzyński, H. Sol, A. Kus, *A&A* **367**, 809–825 (Mar. 2001).
7. M. Chiaberge, G. Ghisellini, *MNRAS* **306**, 551–560 (July 1999).
8. J. L. Gómez, J. M. Martı, A. P. Marscher, J. M. Ibáñez, A. Alberdi, *AJ* **482**, L33–L36 (June 1997).
9. G. Ghisellini, F. Tavecchio, L. Maraschi, A. Celotti, T. Sbarrato, *Nature* **515**, 376–378 (Nov. 2014).
10. J. A. Biretta, W. Junor, M. Livio, *NAR* **46**, 239–245 (May 2002).
11. M. Kadler *et al.*, *AJ* **680**, 867 (2008).
12. T. Beuchert *et al.*, *A&A* **610**, A32 (Feb. 2018).
13. R. Schulz *et al.*, *A&A* **644**, A85 (Dec. 2020).